Supporting Information

A carbon catalyst doped with Co and N derived from the metal-organ-ic framework hybrid (ZIF-8@ZIF-67) for efficient oxygen reduction reaction

ZHANG Ya-ting[1,2,*], LI Si-yi[1,2], ZHANG Na-na[1,2], LIN Gang[1,2], WANG Rui-qi[1,2], YANG Meng-nan[1,2], LI Ke-ke[1,2]

（1. College of Chemistry and Chemical Engineering, Xi'an University of Science and Technology, Xi'an 710054, China;
2. Key Laboratory of Coal Resources Exploration and Comprehensive Utilization, Ministry of Natural Resources, Xi'an 710021, China）

Corresponding author:
ZHANG Ya-ting, Ph. D. Professor. E-mail: isyating@163.com

1. Characterizations

The morphology of the catalysts was inspected using scanning electronic microscopy (SEM, Sirion 200) and transmission electronic microscopy (TEM, JEOL, JEM-2100). X-ray diffraction (XRD) patterns were obtained by a MiniFlex-600 diffractometer. The Raman spectra were collected on an in Via Reflex spectrometer with 532 nm laser excitation. The Brunauer-Emmett-Teller (BET) surface area and the pore size distribution were recorded by nitrogen adsorption-desorption isotherms on a quantachrome adsorption apparatus. The X-ray photoelectron spectroscopy was implemented by virtue of the ThermoFisher K-Alpha instrument.

2. Electrochemical performance evaluation

All electrochemical experiments were implemented employing a three-electrode system on a pine electrochemical workstation outfitted (Wavedrive 20) with MSR electrode rotator (Pine Instrument Co.,Ltd.) under ambient temperature. First, a dispersion system composed of 4 mg of the prepared catalyst powder, 980 μL of ethanol, and 20 μL of 5 wt% Nafion were sonicated for 30 minutes to obtain a catalyst ink. Next, 10 μL of the catalyst ink was coated onto the working electrodes (RDE or RRDE), and then dried in air. A Glass carbon electrode (GCE) was employed as the working electrode, a platinum wire as the counter electrode, and an Ag/AgCl (KCl, saturated) electrode as the reference electrode. As a comparison, a commercial Pt/C catalyst with the same mass loading was executed for the ORR measurements. According to the Nernst formula: $E_{RHE} = E_{Ag/AgCl} + 0.059 \times pH + 0.197$, all the electrochemical potentials measured on the Ag/AgCl reference electrode were transformed into the RHE scale.

Before the ORR measurement, N_2 or O_2 was flowed into the KOH solution for 30 min to

guarantee that it was saturated with N_2 or O_2, and the catalyst was activated by multiple CV cycles until it generated a stable CV curve. CV curves recorded in an 0.1 M N_2- or O_2- saturated KOH electrolyte with a scanning speed of 50 mV s^{-1}. RDE measurements were conducted by LSV from 0.2 to -1 V versus Ag/AgCl in 0.1 M O_2-saturated KOH with a scan rate of 10 mV s^{-1} at different rotation speeds from 400 to 2500 rpm. The ORR durability was executed by a chronoamperometry experiment in 0.1 M O_2-saturated KOH electrolyte at a stationary potential of 0.60 V versus RHE. The current response collected against time over a period of 21600 s was recorded in 0.1 M O_2 saturated KOH solution at a rotation speed of 1600 rpm.

The number of electrons transferred during the ORR was determined via the Koutecky-Levich (K-L) equations:

$$1/j = \frac{1}{nFkC_{O_2}} + \frac{1}{0.62nFAC_{O_2}D_{O_2}^{2/3}V^{-1/6}\omega^{1/2}} \quad (1)$$

Where the kinematic current density, j_k= ¼nFAKC_{O2}. n refers to the transferred electron number per oxygen molecule. F represents the Faraday constant (F= 96485 C mol^{-1}). A is the area of the electrode (0.196 cm^2). C_{O2} refers to the bulk concentration of O_2 (1.2 ×10^{-6} mol cm^{-3}). D_{O2} is the diffusion coefficient of O_2 in 0.1 M KOH at room temperature (1.9 × 10 $^{-5}$ cm^2 s^{-1}). v refers to the kinematic viscosity (0.01 cm^2 s^{-1}). ω corresponds to the rotational speed of the electrode in radians per second (2π rpm/60).

The RRDE test was implemented via LSV from 0.2 to -1 V versus Ag/AgCI with a scanning speed of 10 mV s^{-1} at 1600 rpm. Meanwhile the ring electrode was maintained at 1.3 V versus RHE. The number of transferred electrons (n) and the percentage of hydrogen peroxide (H_2O_2) were counted by using the following formula: $n = 4 \times I_d /(I_d + I_r/N)$ (2) and H_2O_2 (%) = 200 × $(I_r/N)/(I_d + I_r/N)$ (3), where I_d refers to the disk current, I_r refers to the ring current, and N

symbolizes the collection coefficient of the platinum wire (N = 0.37).

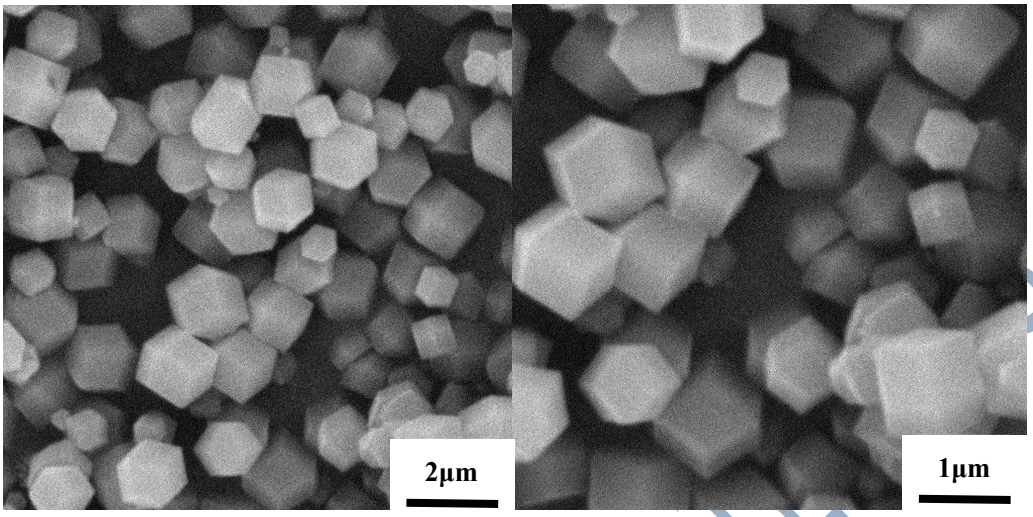

Fig. S1. SEM images of (a,b) ZIF-67.

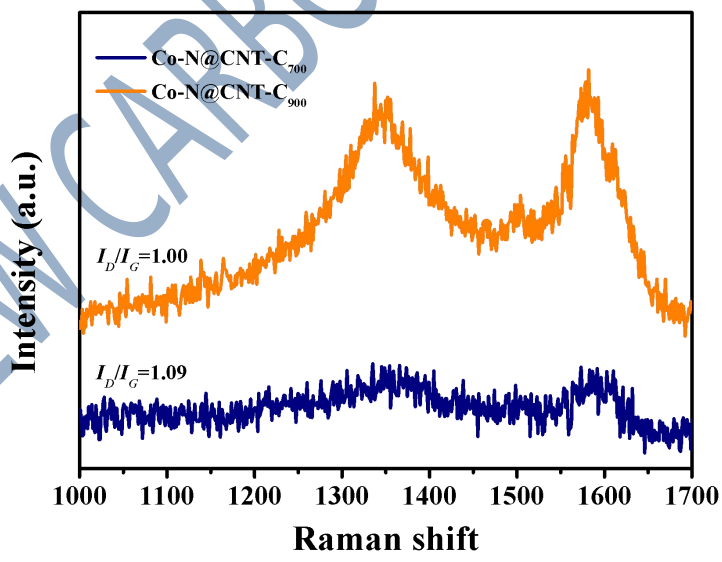

Fig. S2. Raman spectra of Co-N@CNT-C_{700} and Co-N@CNT-C_{700}.

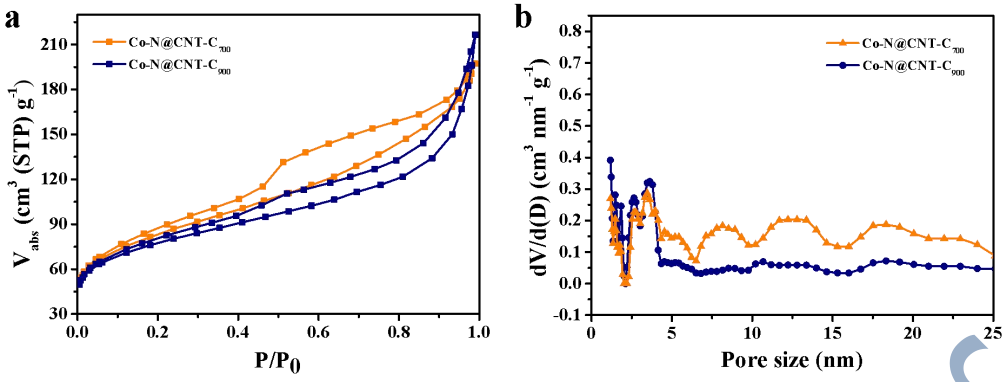

Fig. S3. (a) N_2 sorption isotherms of Co-N@CNT-C_{700} and Co-N@CNT-C_{900}, (b)The pore size distribution corresponding to the Co-N@CNT-C_{700} and Co-N@CNT-C_{900}

Table S1 Summary of the specific surface area, pore volume and average pore size of various samples

samples	BET surface area (m^2 g^{-1})	Average pore size (nm)
Co-N@CNT-C_{800}	428	3.491
C-ZIF-8_{800}	243	3.481
C-ZIF-67_{800}	377	3.111
Co-N@CNT-C_{700}	284	3.969
Co-N@CNT-C_{900}	259	3.104

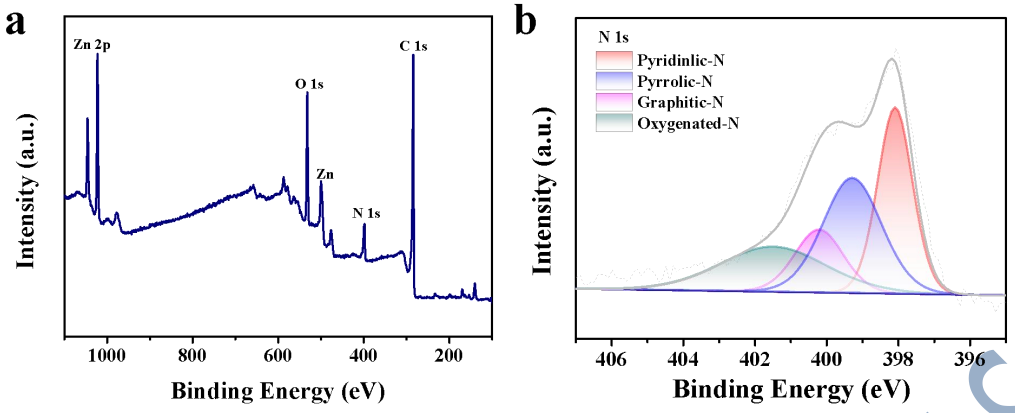

Fig. S4. XPS spectra of C-ZIF-8_{800}. (a) survey. (b) N 1s.

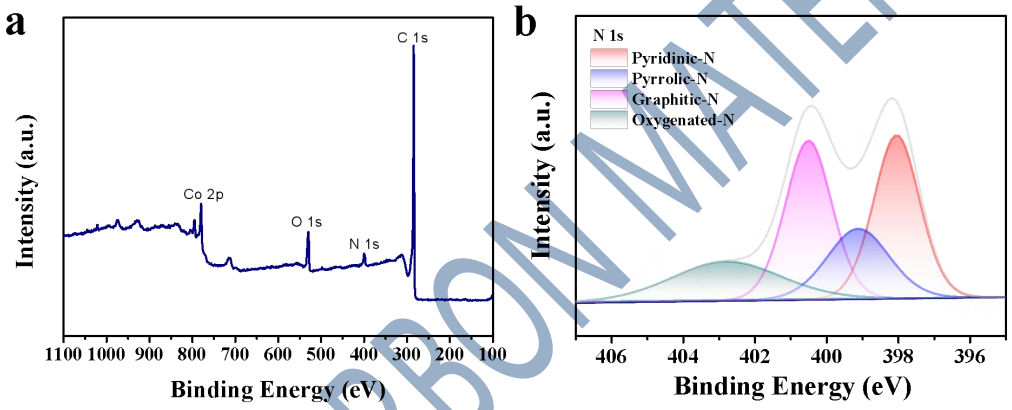

Fig. S5. XPS spectra of C-ZIF-67_{800}. (a) survey. (b) N 1s.

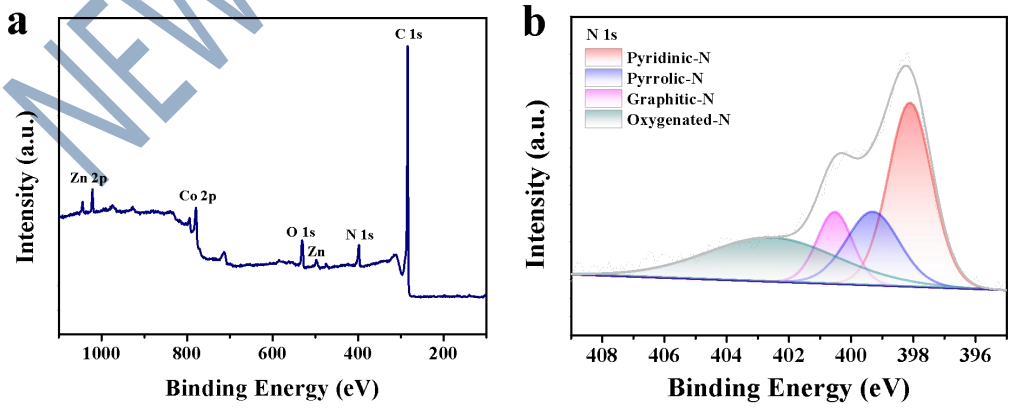

Fig. S6. XPS spectra of C-N@CNT-C_{700}. (a) survey. (b) N 1s.

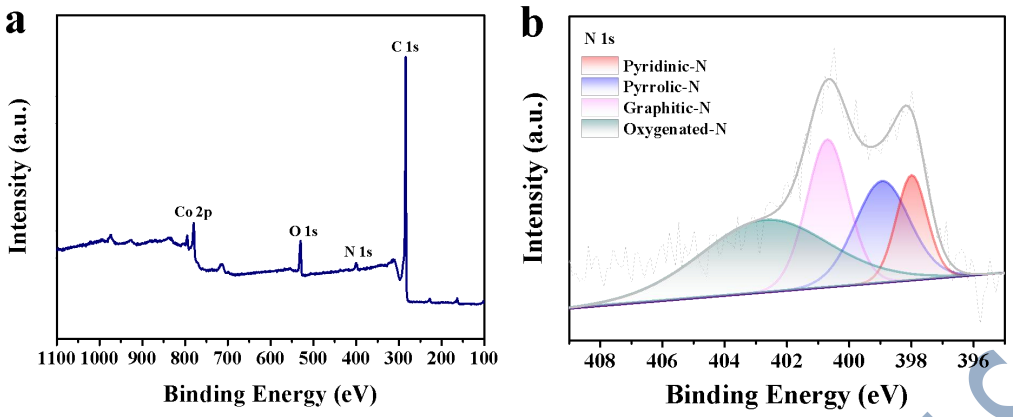

Fig. S7. XPS spectra of C-N@CNT-C_{900}. (a) survey. (b) N 1s.

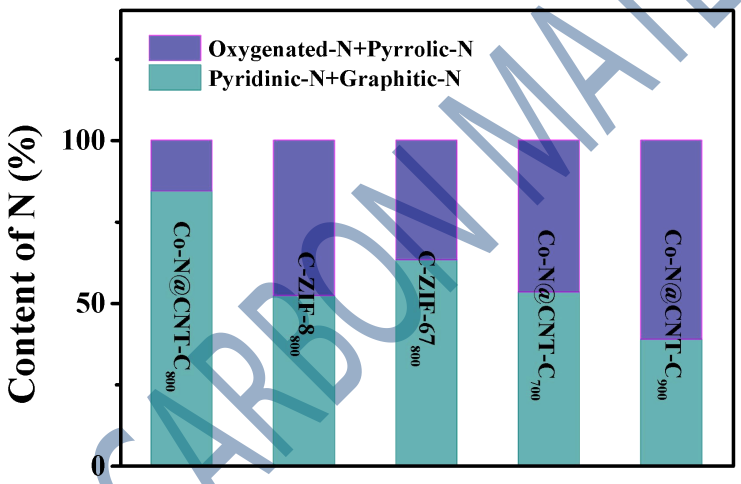

Fig. S8. Content and type of N of all samples

Tab. S2 N1s peak fitting results of all catalysts

samples	Pyridinic-N	Pyrrolic-N	Graphitic-N	Oxygenated-N
Co-N@CNT-C_{800}	42.97	12.41	41.83	2.94
C-ZIF-8_{800}	39.53	19.17	12.67	28.63
C-ZIF-67_{800}	31.83	18.52	31.42	18.23
Co-N@CNT-C_{700}	34.66	20.05	18.65	26.64
Co-N@CNT-C_{900}	13.41	22.83	25.37	38.39

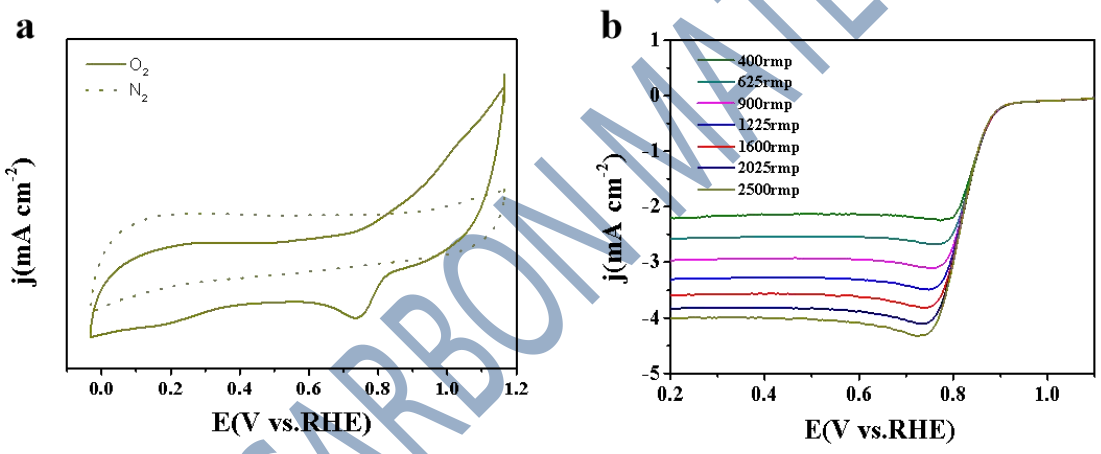

Fig. S9. (a) CVs of C-N@CNT-C_{700} in 0.1 M O_2/N_2-saturated KOH electrolyte (scanning rate: 50 mV s-1). (b) LSV curves of C-N@CNT-C_{700} in 0.1 M O_2-saturated KOH electrolyte at different rotational speeds (from 400 to 2500 rpm) (scanning rate: 10 mV s-1).

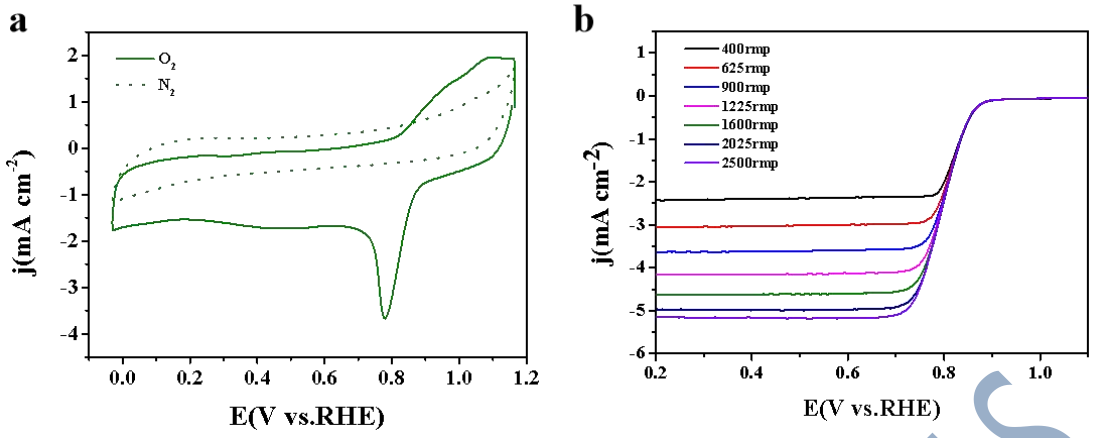

Fig. S10. (a) CVs of C-N@CNT-C_{900} in 0.1 M O_2/N_2-saturated KOH electrolyte (scanning rate: 50 mV s-1). (b) LSV curves of C-N@CNT-C_{900}°C in 0.1 M O_2-saturated KOH electrolyte at different rotational speeds (from 400 to 2500 rpm) (scanning rate: 10 mV s^{-1}).

Table. S3. Comparison of ORR performance of this work with recently reported similar catalysts in alkaline medium.

Entry	Catalyst	E_{onset} (V)	$E_{half\text{-}wave}$ (V)	Reference	Ref
1	Fe_7C_3@FeNC	0.96	0.83	ACS Sustainable Chem. Eng. 2019	[1]
2	Co@N-CNTF-2	0.91	0.81	J. Mater. Chem. A 2019	[2]
3	Co–N–C@F127		0.84	Energ. Environ. Sci. 2019	[3]
4	CoNCF-1000-80	0.92	0.83	Small 2018	[4]
5	Co/CoP–HNC	0.94	0.83	Mater. Horiz. 2018	[5]
6	Co/N CCPC-3	0.921	0.827	Nano Energy	[6]
7	Co/CoP–HNC	0.94	0.83	Mater. Horiz. 2018	[7]
8	Co−N/CNFs	0.94	0.83	ACS Catal. 2017	[8]
9	C-MOF-C2-900		0.817	Adv. Mater. 2018	[9]
10	LDH@ZIF-67-800	0.94	0.83	Adv. Mater. 2016	[10]
11	Fe-N-CC	0.94	0.83	ACS Nano 2016	[11]
12	Fe_2P(3 nm)@BC	0.96	0.83	J. Power Sources 2019	[12]
13	Co-N@CNT-C_{800}	0.94	0.84		This work

Table. S4. Co and Zn atom quantification determined by using inductively coupled plasma optical emission spectroscopy (ICP-OES) as function of Co-N@CNT-C_{800}, C-ZIF-8_{800} and C-ZIF-67_{800}.

Wt%	Co-N@CNT-C_{800}	C-ZIF-8_{800}	C-ZIF-67_{800}
Co	21.79	16.84	0
Zn	0.17	0	23.36

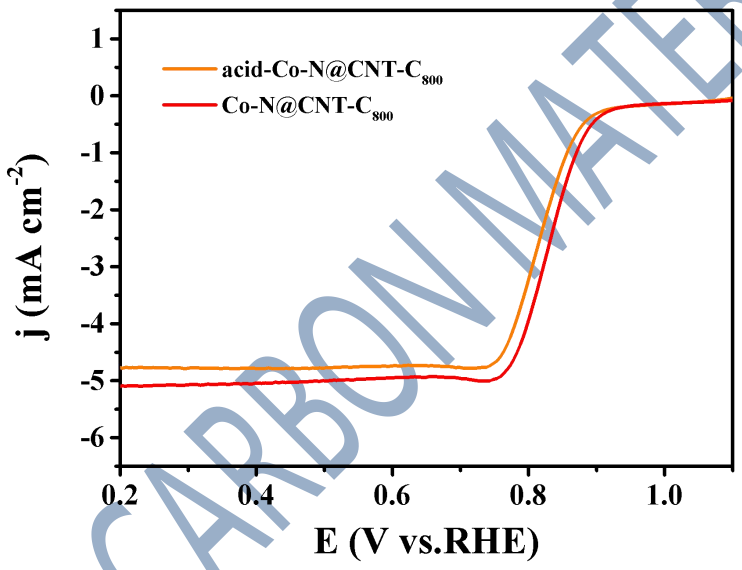

Fig. S11. LSV curves of Co-N@CNT-$C8_{00}$, and acid-Co-N@CNT-C_{800} in O_2-saturated 0.1 M KOH solution.

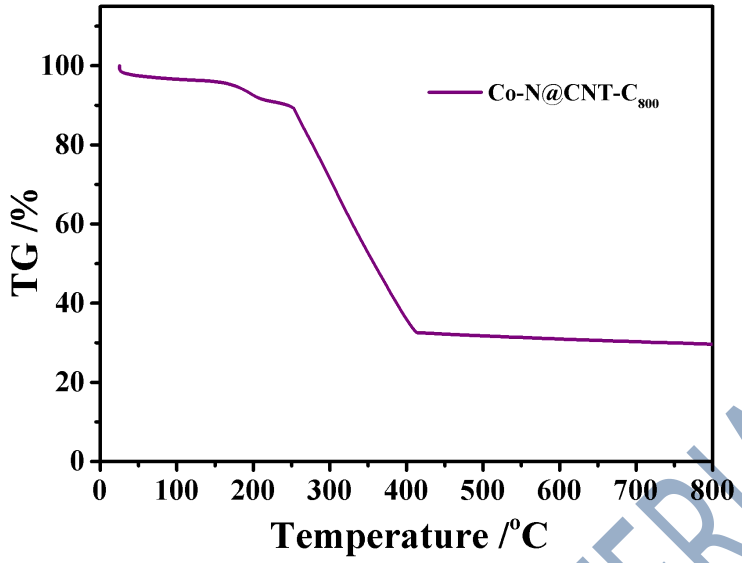

Fig. S12. TGA curves of Co-N@CNT-C_{800} under flowing Air.

	Ⅰ	Ⅱ	Ⅲ	Ⅳ
树脂 (23%)	20.0g	20.0g	20.0g	20.0g
偶氮二异丁腈 (AIBN)	0.06g (1.30%)	0.06g (1.30%)	0.06g (1.30%)	0.055g (1.20%)
ZDA/TPN=1:1	0.06g (1.30%)			
二甲基丙烯酸锌		0.05g (1.09%)		
三烯丙基异氰脲酸酯			0.06g (1.30%)	
三烯氰酸三烯丙酯				0.06g (1.20%)

	Ⅰ	Ⅱ	Ⅲ	Ⅳ	Ⅴ
树脂 (23%)	20.0g	20.0g	20.0g	20.0g	20.0g
偶氮二异丁腈 (AIBN)	0.0192g (0.4%)	0.0192g (0.4%)	0.0192g (0.4%)	0.0192g (0.4%)	0.0192g (0.4%)
二甲基丙烯酸锌	0.0144g (0.3%)	0.0144g (0.3%)	0.0144g (0.3%)	0.0144g (0.3%)	0.0144g (0.3%)
异辛酸锡	0.384g (8.0%)	0.384g (7.8%)	0.384g (8.2%)	0.384g (7.5%)	0.384g (8.5%)

Reference

[1] Niu Y, Teng X, Wang J, Liu Y, Guo L, Song W, et al. Space-Confined Strategy to Fe_7C_3 Nanoparticles Wrapped in Porous Fe-/N-Doped Carbon Nanosheets for Efficient Oxygen Electrocatalysis. ACS Sustainable Chemistry & Engineering 2019;7:13576-83.

[2] Guo H, Feng Q, Zhu J, Xu J, Li Q, Liu S, et al. Cobalt nanoparticle-embedded nitrogen-doped carbon/carbon nanotube frameworks derived from a metal–organic framework for tri-functional ORR, OER and HER electrocatalysis. Journal of Materials Chemistry A 2019;7:3664-72.

[3] He Y, Hwang S, Cullen D A, Uddin A, Langhorst L, Li B, et al. Highly active atomically dispersed CoN_4 fuel cell cathode catalysts derived from surfactant-assisted MOFs: carbon-shell confinement strategy. Energy & Environmental Science 2019,12:250-260.

[4] Jiang H, Liu Y, Li W, Li J. Co Nanoparticles Confined in 3D Nitrogen-Doped Porous Carbon

Foams as Bifunctional Electrocatalysts for Long-Life Rechargeable Zn-Air Batteries. Small 2018;14:1703739.

[5] Hao Y, Xu Y, Liu W, Sun X. Co/CoP embedded in a hairy nitrogen-doped carbon polyhedron as an advanced tri-functional electrocatalyst. Materials Horizons 2018;5:108-15.

[6] Wang T, He Y, Liu Y, Guo F, Li X, Chen H, et al. A ZIF-triggered rapid polymerization of dopamine renders Co/N-codoped cage-in-cage porous carbon for highly efficient oxygen reduction and evolution. Nano Energy 2021;79:105487.

[7] Y.C. Hao, Y.Q. Xu, W. Liu, X.M. Sun, Co/CoP embedded in a hairy nitrogen-doped carbon polyhedron as an advanced tri-functional electrocatalyst, Mater. Horiz. 5 (2018) 108-115.

[8] Q.Q. Cheng, L.J. Yang, L.L. Zou, Z.Q. Zou, C. Chen, Z. Hu, H. Yang, Single Cobalt Atom and N Codoped Carbon Nanofibers as Highly Durable Electrocatalyst for Oxygen Reduction Reaction, ACS Catal. 7 (2017) 6864-6871.

[9] M.D. Zhang, Q.B. Dai, H.G. Zheng, M.D. Chen, and L.M. Dai, Novel MOF-Derived Co@N-C Bifunctional Catalysts for Highly Efficient Zn-Air Batteries and Water Splitting, Adv. Mater. 30 (2018) 1705431.

[10] Z.H. Li, M.F. Shao, L. Zhou, R.K. Zhang, C. Zhang, M. Wei, D.G. Evans, X. Duan, Directed Growth of Metal-Organic Frameworks and Their Derived Carbon-Based Network for Efficient Electrocatalytic Oxygen Reduction, Adv. Mater. 28 (2016) 2337-2344.

[11] G.A. Ferrero, K. Preuss, A. Marinovic, A.B. Jorge, N. Mansor, D.J.L. Brett, A.B. Fuertes, M. Sevilla, M.-M. Titirici, Fe–N-doped carbon capsules with outstanding electrochemical performance and stability for the oxygen reduction reaction in both acid and alkaline conditions, ACS nano 10 (2016) 5922-5932.

[12] Y.L. Ye, W.J. Duan, X.Y. Yi, Z.C. Lei, Ge Li, C.H. Feng, Biogenic precursor to size-controlled synthesis of Fe_2P nanoparticles in heteroatom-doped graphene-like carbons and their electrocatalytic reduction of oxygen, J. Power Sources 435 (2019) 226770.